Current Harmonics in Surface-Mounted PMSM Electrical Drive for Monitoring Torsional Vibrations

Dejan Pejovski, Antonino Di Gerlando, *Senior Member, IEEE*, Giovanni Maria Foglia, Matteo Felice Iacchetti, *Senior Member, IEEE*, and Roberto Perini, *Member, IEEE*

***Abstract*—Electromagnetic torque harmonics commonly exist in electrical drives due to inverter modulation, current harmonic propagation, etc. They excite torsional vibrations on the shaft which are reflected in the electrical quantities, such as stator line currents. In this paper, the existence of current harmonics originating from both voltage harmonics due to inverter modulation and mechanical oscillations in a surface-mounted permanent magnet synchronous machine (SPMSM) drive is analysed in depth. An analytical model which can accurately predict current harmonic amplitudes is presented. The theoretical development is also useful for detecting incipient torsional resonance or for identifying the natural frequencies of the electrical drive, both analytically and experimentally. An experimental setup consisting of a 6.9 kW SPMSM coupled to a dc generator is used to validate the theoretical studies.**

***Index Terms*—Vibrations control, torsional resonance, PWM harmonic, shaft torque harmonic, resonant frequency.**

I. Introduction

ELECTRICAL drives are subject to mechanical vibrations originating from mechanical and electrical sources [1]. The most common causes of torsional vibrations are perturbations in the motor power supply [2], non-sinusoidal back-emf [3], mechanical imperfections (shaft misalignment, eccentricity [4]), load oscillations, bearing and/or gearbox faults [5], slip-stick phenomenon [6]. In a variable frequency drive, torsional vibrations increase audible noise [7], accelerate shaft fatigue, reduce the drive-train lifetime, and can cause mechanical damage with shaft breakdown as the worst outcome [8]. Therefore, understanding and monitoring the vibrations, as well as applying suitable damping techniques is essential for any electrical drive.

Various techniques have been employed for measuring torsional vibrations beyond the common ones (strain gauges, torque meters) [9]. Recently, a wireless on-shaft unit with high performances has been proposed for online vibration monitoring [10]. Another non-invasive method consists in using the electromagnetic torque signature [11], or the cogging torque for stator circumferential vibration [12]. Since measuring the air-gap torque directly is not easy, estimating it from measured voltages, currents and estimated resistance is proposed [11]. The stator current harmonics are often used as an indicator of torsional vibrations and mechanical faults. The current envelope, combined with a time-frequency analysis, provides sufficient details for monitoring torsional vibration due to gearbox faults [13], blade imbalance [14], load torque oscillations [15]. Current signature is also used for identifying bearings defects [16] and inter-turn faults [17]. A thorough analysis of the torsional vibrations in a permanent-magnet (PM) machine drive is presented in [18]. However, neither a methodology nor guidelines are proposed to compute the amplitude of the current harmonics.

All the above-mentioned papers assume a mechanical torque harmonic at a frequency f_m which, regardless of its origin, is reflected on the electrical side giving rise to two current harmonics at frequencies $|f_1 \pm f_m|$ (current “paired” harmonics), f_1 being the fundamental frequency of the supply voltage. A detailed graphical representation of the relationship between mechanical and electrical quantities and the corresponding frequencies is given in [19]. On the other hand, a simple analytical model is presented in [20], regarding both SPMSM and induction machine. It was experimentally proved that the amplitudes of these paired current harmonic components change proportionally to the twisting torque, enabling dynamic monitoring of the shaft torsional vibration. Reference [20], however, does not analyse how the individual amplitude of each paired harmonic changes with frequency. In [21], the machine model was modified to account for a ripple in the rotor speed and predict the line current harmonics. However, the procedure is iterative, it refers to an induction machine only, and does not consider the mechanical coupling between the motor and the drivetrain. In [22], torque and speed harmonic quadrature magnitudes are related to a pair of harmonic current quadrature amplitudes by a unique relationship that accounts for stator copper losses. However, the model uses a one Degree-of-Freedom (DOF) mechanical system, which is not suitable for analysing torsional vibrations. In [2], a multiple synchronous rotating frames-based drive model is employed to obtain a relationship between injected voltage and resulting current harmonic: this relation depends on motor speed and drive control. This approach involves low-pass filters and additional

Manuscript received Month xx, 2xxx; revised Month xx, xxxx; accepted Month x, xxxx.
The authors are with the Department of Energy, Politecnico di Milano, 20156 Milano, Italy (e-mail: dejan.pejovski@polimi.it; antonino.digerlando@polimi.it; gianmaria.foglia@polimi.it; matteo.iacchetti@polimi.it; roberto.perini@polimi.it). Matteo F. Iacchetti is also with the School of Engineering of The University of Manchester – Manchester, UK.

controllers which cause delays and stability problems, especially in presence of speed harmonics, as shown in [23].

The existing literature exhibits some gaps which need addressing:

1) no complete analytical model of a SPMSM drive including the voltage-source inverter (VSI) and mechanical load is available to predict current harmonic amplitudes due to voltage harmonic excitation near mechanical resonance;
2) no comprehensive explanation can be found for the origin of paired current harmonics due to a single voltage harmonic and for their correlation with electromagnetic and shaft torque components;
3) overlook in the interpretation of current harmonic amplitude behaviour around critical operating points.

This paper will present a comprehensive model of an SPMSM electrical drive at torsional resonance. A voltage harmonic originating from VSI modulation gives rise to current and, consequently, torque harmonics. The paper will explain in detail how this voltage harmonic propagates through the control and affects the overall drive response. The proposed model can predict current "paired" harmonics at mechanical resonance: their amplitudes vary with the operating conditions (speed and load) and hence, can be used to forecast torsional resonance.

The main contributions are:

1) An all-inclusive 7th-order mathematical model of an electrical drive including speed/current control, SPMSM electrical equations and 2DOF mechanical model to describe drive's behaviour at torsional resonance;
2) Prediction of electromagnetic and shaft torque harmonics as well as paired current harmonics at resonance originating from VSI modulation;
3) Novel interpretation of the amplitude similarity between torque and current harmonics at resonance;
4) Analysis of the effect of load torque, inertia and current loop bandwidth on the model robustness as well as on the torsional resonance severity.

Torsional resonance can be detected by monitoring the shaft torque waveform acquired by a torque meter, that is not typically employed in electrical drives. Among the model advantages highlighted in this paper is the possibility to predict the resonance by monitoring only the line current.

The paper is organised as follows. The analytical model is presented in Sec. II. An extensive sensitivity analysis is performed in Sec. III. In Sec. IV an experimental setup consisting of a 6.9 kW SPMSM machine coupled with a dc generator which supplies a passive load is used to validate the theoretical model. Conclusions are presented in Sec. V.

II. Analytical Model of an SPMSM Drive

A. Assumptions

The electrical drive considered in this paper is shown in Fig. 1 and consists of a SPMSM coupled to a load and supplied by a VSI. To describe the drive mathematically by suitable differential equations, the following assumptions are made:

1) The machine is a surface-mounted PM one (thus, $L_d = L_q = L$), with nearly-sinusoidal air-gap flux density distribution, and constant PM flux linkage Ψ_{PM}, n_p pole pairs and resistance R.
2) Magnetic saturation as well as the effect of the stator teeth and slots on the air-gap torque are neglected.
3) Mechanical coupling is non-ideal, i.e. the joint has finite stiffness K and non-zero damping B; the motor and load moments of inertia J_m, J_L are considered separately.
4) Decoupled inner current and outer speed control based on PI regulators (parameters k_{pI}, k_{iI}, $k_{p\Omega}$, $k_{i\Omega}$) are used, enforcing maximum-torque-per-ampere conditions.

Regardless of the modulation technique, the SPMSM supply voltage will contain harmonic components [24], which generate current harmonics, and consequently torque ripple. This causes oscillations of the rotor angular position and machine speed [25], which are fed back to the control. The sinusoidal oscillation, superposed to the constant terms in the SPMSM dynamical model in the *dq*-frame, leads to a nonlinear system [26], which is linearized around a steady-state operating point.

B. Mathematical Model

The system in Fig. 1 is based on a second-order electrical machine model, a second-order mechanical model and a third-order control model.

The machine model in the αβ-frame is ($p=d/dt$):

$$\overline{v}_{\alpha\beta}^{ref} + \overline{v}_{\alpha\beta(h_v)}^{dist} = R\,\overline{i}_{\alpha\beta} + p\overline{\Psi}_{\alpha\beta} \tag{1}$$

The quantity $\overline{v}_{\alpha\beta(h_v)}^{dist}$ denotes a generic harmonic voltage input disturbance of order h_v deemed to arise in the *abc*-frame as a result of the inverter modulation (either due to switching or overmodulation).

$$v_{abc(h_v)}^{dist} = \hat{V}_h \cos\left(h_v\left(\omega_1 t + 0; -120°; +120°\right)\right), \tag{2}$$

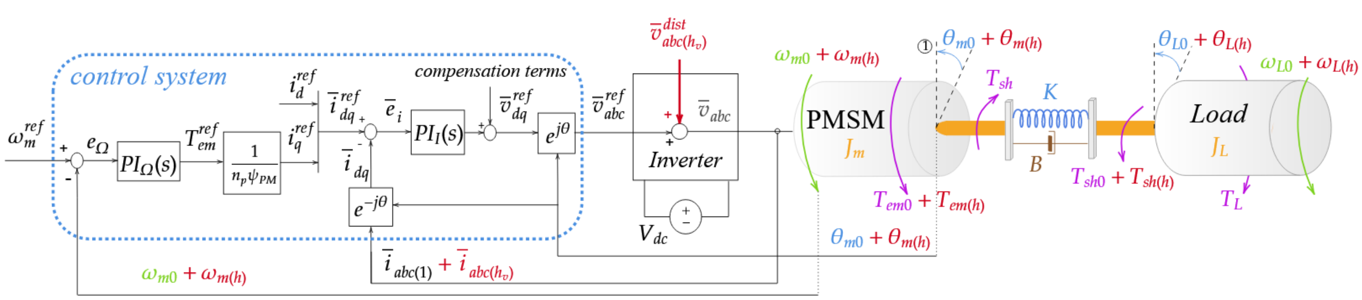

Fig. 1. System under study: electrical drive consisting of a dc power source, VSI, PMSM, load and control system.

where ω_1 is the fundamental angular frequency. These are treated as "inputs" and their mapping into the dq-frame will be explained in Sect. II.C. Voltage $\bar{v}_{\alpha\beta}^{ref}$ represents the voltage imposed by the current controllers and may include harmonics propagated through the control.

The mechanical model is a second-order one (Fig. 1), where viscous damping torque $B_m\omega_m$ and $B_L\omega_L$ are usually neglected:

$$\begin{cases} J_m\, p\omega_m = T_{em} - K(\theta_m - \theta_L) - B(\omega_m - \omega_L) - B_m\omega_m \\ J_L\, p\omega_L = K(\theta_m - \theta_L) + B(\omega_m - \omega_L) - T_L - B_L\omega_L \end{cases} \quad (3)$$

The control system in a dq-frame consists of current and speed PI controllers:

$$p\varepsilon_{id} = i_d^{ref} - i_d\,;\; p\varepsilon_{iq} = i_q^{ref} - i_q\,;\; p\varepsilon_{\Omega} = \omega_m^{ref} - \omega_m \quad (4)$$

$$\begin{cases} v_d^{ref} = k_{pI}\left(i_d^{ref} - i_d\right) + k_{iI}\,\varepsilon_{id} - n_p\omega_m L i_q \\ v_q^{ref} = k_{pI}\left(i_q^{ref} - i_q\right) + k_{iI}\,\varepsilon_{iq} + n_p\omega_m\left(\psi_{PM} + L i_d\right) \\ T_{em}^{ref} = k_{p\Omega}\left(\omega_m^{ref} - \omega_m\right) + k_{i\Omega}\varepsilon_{\Omega} \end{cases} \quad (5)$$

The inverter is represented by a time constant T_{sw}.

$$\bar{v}_{dq} = (1 + pT_{sw})^{-1}\, \bar{v}_{dq}^{ref} \quad (6)$$

By applying the small signal analysis about a steady-state condition (subscript 0), the following model in matrix form derives, linking up the control part with the electrical and mechanical drive dynamics (1)-(6) (see [1] for further details):

$$s \cdot \Delta x = \boldsymbol{A_{sys}} \cdot \Delta x + \boldsymbol{B_u} \cdot \Delta u \quad (7)$$

where $\boldsymbol{A_{sys}}$ (6x6) and $\boldsymbol{B_u}$ (6x2), as given in (8), are system and control input matrices, respectively, s is the Laplace variable, Δx is the vector of state variables variations and Δu is the vector of inputs (Sect. II.C), as given in (9).

$$\Delta x = \left\{\Delta\psi_d \quad \Delta\psi_q \quad \Delta\omega \quad \Delta\varepsilon_{id} \quad \Delta\varepsilon_{id} \quad \Delta\varepsilon_{\Omega}\right\}^T$$
$$\Delta u = \left\{\Delta v_d \quad \Delta v_q\right\}^T \quad (9)$$

where $\Delta\psi_d$ and $\Delta\psi_q$ are flux variations, $\Delta\omega$ is motor electrical speed variation, $\Delta\varepsilon_{id}$, $\Delta\varepsilon_{iq}$ and $\Delta\varepsilon_{\Omega}$ are variations of the controller integral errors.

Solving (7) yields transfer functions $G_{out}^{in}(s)$ between the inputs ($in = \Delta i_d$, Δi_q) and the state variables ($out = \Delta\psi_d$, $\Delta\psi_q$, $\Delta\omega$). Hence, each state variable variation depends on two terms, related to both inputs:

$$\begin{cases} \Delta\psi_d(s) = G_{\Delta\psi_d}^{\Delta v_d}(s)\Delta V_d(s) + G_{\Delta\psi_d}^{\Delta v_q}(s)\Delta V_q(s) \\ \Delta\psi_q(s) = G_{\Delta\psi_q}^{\Delta v_d}(s)\Delta V_d(s) + G_{\Delta\psi_q}^{\Delta v_q}(s)\Delta V_q(s) \\ \Delta\omega(s) = G_{\Delta\Omega}^{\Delta v_d}(s)\Delta V_d(s) + G_{\Delta\Omega}^{\Delta v_q}(s)\Delta V_q(s) \end{cases} \quad (10)$$

Current variations Δi_d and Δi_q are simply $\Delta i_{dq} = \Delta\psi_{dq} / L$.

C. Inputs Δu of the system in the dq-frame

It is assumed that, due to the voltage harmonic $\bar{v}_{\alpha\beta(h_v)}^{dist}$, the motor angular speed oscillates about its steady state value and thus the electrical angle θ is as follows:

$$\theta = \omega_1 t + \hat{\theta}_h sin(h\omega_1 t - \varphi_{\Omega,h}) = \omega_1 t + \Delta\theta^{dist}, \quad (11)$$

where $\hat{\theta}_h$ is the ripple amplitude. Positive and negative sequence harmonics produce $h=h_v-1$ and $h=h_v+1$, respectively.

To map disturbance voltage (2) into the dq-frame, one can linearise operator $exp(-j\theta)$ with respect to ripple amplitude $\hat{\theta}_h$:

$$e^{-j\theta} = e^{-j\omega_1 t - j\Delta\theta^{dist}} \approx e^{-j\omega_1 t}\left(1 - j\hat{\theta}_h \sin\left(h\omega_1 t - \varphi_{\Omega,h}\right)\right) \quad (12)$$

Applying the power-invariant Park transform to $\bar{v}_{\alpha\beta(h_v)}^{dist}$ in (2) with (11) and (12), and ignoring 2nd-order vanishing terms such as "$V_h\hat{\theta}_h$" yields:

$$\bar{v}_{dq(h_v)}^{dist}(t) = \bar{v}_{\alpha\beta(h_v)}^{dist}(t)\, e^{-j\,\theta(t)} = \dots$$
$$= +\sqrt{3/2}\,\hat{V}_h\left\{cos\left(h\omega_1 t\right) + j sin\left(h\omega_1 t\right)\right\} \quad (13)$$

where $h=h_v \mp 1$ for positive/negative sequence.

So, it can be assumed that the input voltage variations due to $\bar{v}_{\alpha\beta(h_v)}^{dist}$ disturbance are:

$$\begin{aligned} \Delta v_d &= \sqrt{1.5}\hat{V}_h \cos\left(h\omega_1 t\right) \\ \Delta v_q &= \sqrt{1.5}\hat{V}_h\, sin\left(h\omega_1 t\right), \end{aligned} \quad (14)$$

$$\boldsymbol{A_{sys}} = \begin{bmatrix} -\frac{R}{L} - \frac{k_{pI}}{L(1+sT_{sw})} & \frac{sT_{sw}}{1+sT_{sw}}\omega_0 & \frac{sT_{sw}}{1+sT_{sw}}\psi_{q0} & \frac{k_{iI}}{1+sT_{sw}} & 0 & 0 \\ -\frac{sT_{sw}}{1+sT_{sw}}\omega_0 & -\frac{R}{L} - \frac{k_{pI}}{L(1+sT_{sw})} & a_{23}(s) & 0 & \frac{k_{iI}}{1+sT_{sw}} & \frac{k_{pI}k_{i\Omega}}{n_p\psi_{PM}(1+sT_{sw})} \\ 0 & a_{32}(s) & 0 & 0 & 0 & 0 \\ -\frac{1}{L} & 0 & 0 & 0 & 0 & 0 \\ 0 & -\frac{1}{L} & -\frac{k_{p\Omega}}{n_p^2\psi_{PM}} & 0 & 0 & \frac{k_{i\Omega}}{n_p\psi_{PM}} \\ 0 & 0 & -\frac{1}{n_p} & 0 & 0 & 0 \end{bmatrix} \quad \boldsymbol{B_u} = \begin{bmatrix} 10 \\ 01 \\ 00 \\ 00 \\ 00 \\ 00 \end{bmatrix} \quad (8)$$

$$a_{32}(s) = \frac{\psi_{PM}}{L} n_p^2 \frac{J_L s^2 + Bs + K}{J_m J_L s^2 + B\left(J_m + J_L\right)s + K\left(J_m + J_L\right)} \quad \text{and} \quad a_{23}(s) = -\frac{sT_{sw}}{1+sT_{sw}}\psi_{d0} - \frac{k_{pI}k_{p\Omega}}{n_p^2\psi_{PM}\left(1+sT_{sw}\right)}$$

where h is the harmonic order in dq-frame.

D. Current harmonics in the abc-frame

By superposing the effects of both inputs Δv_d and Δv_q on the same state variable in the frequency domain, shown in (10), currents Δi_d and Δi_q and the motor electrical speed can be expressed back in the time-domain as:

$$\begin{cases} \Delta i_d = \hat{I}_{dh} \cos\left(h\omega_1 t - \varphi_{id,h}\right) \\ \Delta i_q = \hat{I}_{qh} \cos\left(h\omega_1 t - \varphi_{iq,h}\right), \\ \Delta\omega = \hat{\omega}_h \cos\left(h\omega_1 t - \varphi_{\Omega,h}\right) \end{cases} \tag{15}$$

where amplitudes $\hat{I}_{dh}$, $\hat{I}_{qh}$, and $\hat{\omega}_h$, and phases $\varphi_{id,h}$, $\varphi_{iq,h}$, and $\varphi_{\Omega,h}$ depend on all the parameters in the system matrix $\boldsymbol{A_{sys}}$ and are computed by evaluating the trigonometric sum of the transfer functions in (10) at the exciting frequency $h\omega_1$, as shown in [27].

By taking the magnetic axis of *phase a* as the origin for the rotor angle, the instantaneous line current i_a is computed using (15) and (12):

$$i_a = Re[(\bar{i}_{dq0} + \Delta\bar{i}_{dq})e^{j\theta}] \approx i_{a(1)} + \Delta i_a, \tag{16}$$

where the fundamental component is:

$$i_{a(1)} \approx i_{d0} \cos\left(\omega_1 t\right) - i_{q0} \sin\left(\omega_1 t\right), \tag{17}$$

and the line current ripple Δi_a consists of several terms:

$$\begin{aligned} \Delta i_a \approx{}& \Delta i_d \cos\left(\omega_1 t\right) - \Delta i_q \sin\left(\omega_1 t\right) \\ &- i_{d0}\Delta\theta^{dist} \sin\left(\omega_1 t\right) - i_{q0}\Delta\theta^{dist} \cos\left(\omega_1 t\right). \end{aligned} \tag{18}$$

Each product in (18) gives rise to two current components at frequencies $(h\pm1)\omega_1$, as in (19). Mapping them back into the abc-frame, for a positive sequence voltage disturbance input $v_{abc(h_v)}^{dist}$, results in current harmonics at frequencies $h_v\omega_1$ and $(h_v\text{-}2)\omega_1$, respectively, as per (20). Only one of them matches the disturbance input voltage harmonic order, while the other one is entirely due to the torsional vibration. To compute the corresponding amplitudes I_{hv} and $I_{hv\text{-}2}$, simple trigonometric formulae can be applied to sum up all the components in (19) which contribute to the same current harmonic:

$$\begin{aligned} \Delta i_a \approx{}& \hat{I}_{h_v} \cos\left(h_v\omega_1 t - \varphi_{ia,hv}\right) + \\ &+ \hat{I}_{h_v-2} \cos\left(\left(h_v - 2\right)\omega_1 t - \varphi_{ia,hv-2}\right). \end{aligned} \tag{20}$$

Similarly, for a negative-sequence input harmonic voltage disturbance $\bar{v}_{abc(h_v)}^{dist}$ of order h_v, it is h=h_v+1 and the harmonic pair appears in the line current at frequencies $h_v\omega_1$ and $(h_v+2)\omega_1$ respectively.

Equations (14) to (20) show how a generic harmonic voltage input disturbance $\bar{v}_{abc(h_v)}^{dist}$ of order h_v in the abc-frame generates two paired current harmonics (expressed by (20), if $\bar{v}_{abc(h_v)}^{dist}$ is of positive sequence). A simplified graphical representation of these mathematical steps is shown in Fig. 2. The harmonics resulting from the product of two variations $\Delta x\cdot\Delta y$ are considered negligible.

E. Simplified analytical study

A few simplifying hypotheses help providing some analytical insight on the correlation between torque and current components.

$$\begin{aligned} \Delta i_a \approx 0.5[&\hat{I}_{dh} \cos\left(\left(h-1\right)\omega_1 t - \varphi_{id,h}\right) + \hat{I}_{dh} \cos\left(\left(h+1\right)\omega_1 t - \varphi_{id,h}\right) + \\ &+ \hat{I}_{qh} \sin\left(\left(h-1\right)\omega_1 t - \varphi_{iq,h}\right) - \hat{I}_{qh} \sin\left(\left(h+1\right)\omega_1 t - \varphi_{iq,h}\right) + \\ &- i_{d0}\hat{\theta}_h \cos\left(\left(h-1\right)\omega_1 t - \varphi_{\Omega,h}\right) + i_{d0}\hat{\theta}_h \cos\left(\left(h+1\right)\omega_1 t - \varphi_{\Omega,h}\right) + \\ &- i_{q0}\hat{\theta}_h \sin\left(\left(h-1\right)\omega_1 t - \varphi_{\Omega,h}\right) - i_{q0}\hat{\theta}_h \sin\left(\left(h+1\right)\omega_1 t - \varphi_{\Omega,h}\right)]. \end{aligned} \tag{19}$$

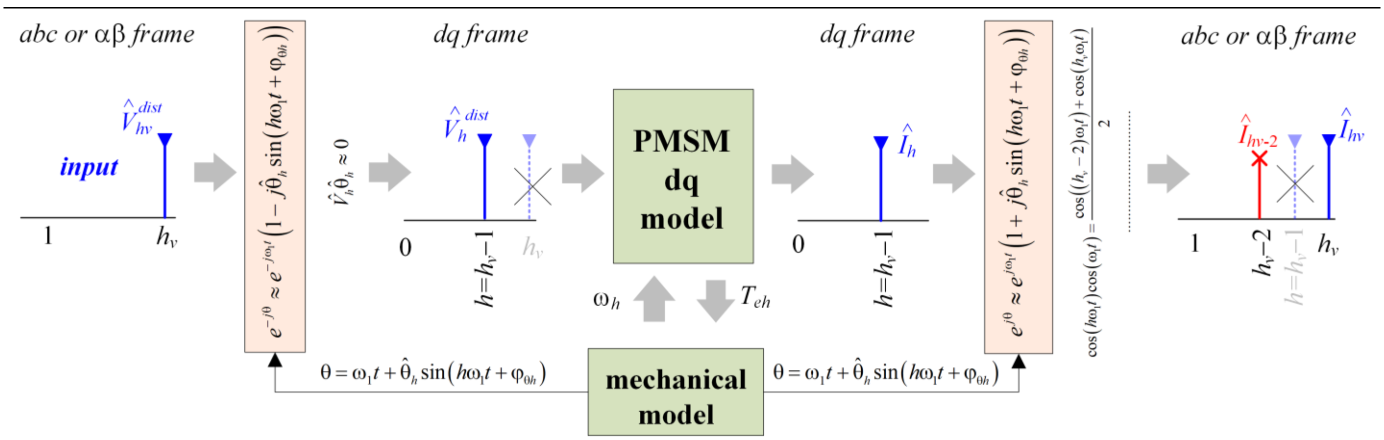

Fig. 2. Generation of paired current harmonics due to a positive sequence voltage harmonic disturbance $\hat{V}_{hv}^{dist}$ in the abc-frame.

With T_{sw}=0 (ideal inverter), i_{d0}=0 (MTPA, maximum torque per ampere strategy), $k_{p\Omega}$= $k_{i\Omega}$=0 (torque control only), B=0 (no mechanical damping), the same procedure as in (10)÷(18) yields:

$$G_{\Delta\psi_d}^{\Delta v_q}(s) = G_{\Delta\psi_q}^{\Delta v_d}(s) = G_{\Delta\Omega}^{\Delta v_d}(s) = 0,$$
$$G_{\Delta\psi_d}^{\Delta v_d}(s) = G_{\Delta\psi_q}^{\Delta v_q}(s), \tag{21}$$

The amplitudes of the dq current harmonic of order h are:

$$\hat{I}_{dh} = \hat{I}_{qh} = \left(\left|G_{\Delta\psi_q}^{\Delta v_q}(s)\right| / L\right)\hat{V}_h$$
$$= \left|\frac{s}{s^2+\left((R+k_{pI})/L\right)s+k_{iI}/L}\right|\hat{V}_h, \tag{22}$$

while the amplitude of the harmonic angular oscillations becomes:

$$\hat{\theta}_h = \left|\frac{\hat{\omega}_h}{s}\right| = \left|\frac{G_{\Delta\Omega}^{\Delta v_q}(s)}{s}\right|\hat{V}_h$$
$$= \frac{n_p^2\,\psi_{PM}}{J_m}\left|\frac{s^2+\omega_{aN,mech}^2}{s^2\left[s^2+\omega_{N,mech}^2\right]}\right|\left|\hat{I}_{qh}\right| \tag{23}$$

$$J_{eq} = \frac{J_m \cdot J_L}{J_m+J_L}, \omega_{aN,mech} = \sqrt{\frac{K}{J_L}}, \omega_{N,mech} = \sqrt{\frac{K}{J_{eq}}}, \tag{24}$$

Transfer function (23) depends on the anti-resonance $\omega_{aN,mech}$ and resonance $\omega_{N,mech}$ angular frequencies and on the current harmonic $\hat{I}_{qh}$, i.e. it has the poles of the current loop.

Now, the line current harmonics are:

$$\Delta i_a \approx \hat{I}_{qh}\cos\left(h_v\omega_1 t+\varphi_{idq}\right)+$$
$$+0.5 i_{q0}\hat{\theta}_h\cos\left(h_v\omega_1 t+\varphi_{\Omega,h}\right)+ \tag{25}$$
$$+0.5 i_{q0}\hat{\theta}_h\cos\left(\left(h_v-2\right)\omega_1 t+\varphi_{\Omega,h}\right)$$

In (25), the current harmonic component of order (h_v-2) depends only on amplitude $\hat{\theta}_h$ of the motor rotor position oscillation, while the $\hat{\theta}_h$-related term in the harmonic current of order (h_v) is largely dominated by the $\hat{I}_{qh}$-term when the system is far from the mechanical resonance. Two key consequences follow.

First, the line current harmonic $I_{(hv)}$ can be approximated by only the first term in (25), hence $I_{(hv)} \sim \Delta i_q$, and, for a SPMSM $T_{em(h)} = n_p \cdot \psi_{PM} \cdot \Delta i_q \sim \Delta i_q \sim \hat{I}_{qh}$. Thus, it can be concluded that the current harmonic of order h_v is proportional to the electromagnetic torque: $I_{(hv)} \sim T_{em(h)}$.

Secondly, the current harmonic component of order (h_v-2) can be considered as representative of the shaft torque T_{sh} and then is a possible indicator of incipient resonance. In fact, from (3), the shaft torque harmonic can be expressed as:

$$T_{sh(h)}(s) = K\left(\theta_{m(h)}(s) - \theta_{L(h)}(s)\right) =$$
$$= \theta_{m(h)}(s) \cdot K \cdot s^2/\left(s^2+\omega_{aN,mech}^2\right) \tag{26}$$

Since transfer function $s^2/\left(s^2+\omega_{aN,mech}^2\right)$ in (26) equals one for $\omega > \omega_{aN,mech}$, the shaft torque harmonic becomes roughly proportional to the motor rotor position harmonic $\theta_{m(h)} = \Delta\theta = \hat{\theta}_h\cos\left(h\omega_1 t+\varphi_{\Omega,h}\right)$. Regarding the line current harmonic $I_{(hv-2)}$ given by the last term in (25), it is obviously proportional to $\hat{\theta}_h$. Hence, $I_{(hv-2)} \sim T_{sh(h)}$.

A simplified flowchart of the method proposed in Sect. II is shown in Fig. 3 to ease procedure understanding.

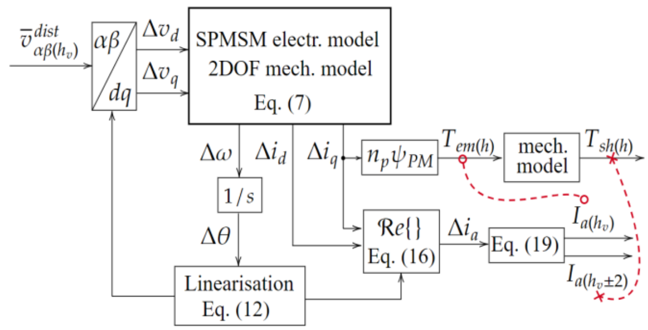

Fig. 3. Simplified flowchart of the proposed analytical method for computing paired line current harmonics at resonance originating from a voltage harmonic. Dashed lines highlight amplitude trend correlations between the variables.

III. Sensitivity Analysis and Discussion

To highlight the correlation between current and torque harmonics an in-depth sensitivity analysis based on the proposed analytic model was carried out using the data of an experimental setup (Sect. IV) with electrical and mechanical drive parameters as given in Appendix I. The switching frequency was f_{sw}=5kHz. The mechanical resonant angular frequency (24) is $\omega_{N,mech}$=2π·158.5rad/s – see Fig. 11 in Section IV. Thus, as a baseline scenario, the speed-loop cut-off frequency was set at a much lower value – i.e. $f_{c,\Omega}$=0.1Hz – to avoid instability caused by the phase lag due to the resonance peak, while the current loop cut-off frequency was set at $f_{c,I}$=300Hz. For any value of the load torque and, thus, of current i_{q0}, the overall natural frequency due to the mechanical and control system interaction [27] is practically equal to $\omega_{N,mech}$.

Both in the following evaluations and in the experimental tests, we injected a positive-sequence harmonic voltage disturbance $\overline{v}_{\alpha\beta(h_v)}^{dist}$ of order h_v=13 and amplitude V_h=0.2 p.u. into the VSI reference voltages. We swept the fundamental frequency over a range so that the resulting frequency range for harmonic h_v included the mechanical resonant frequency $f_{N,mech}$. We recorded the amplitude trends of torque harmonics of order h=h_v-1=12 and current harmonics h_v=13 (originating from the voltage harmonic input) and h_v-2=11 (entirely due to torsional resonance). We repeated these fundamental-frequency sweeps for different current i_{q0}, load inertia J_L and current loop cut-off frequency $f_{c,I}$ values.

All the plots in this Section are obtained in Wolfram Mathematica by using the analytical model proposed in Sect. II. Simulations were carried out by Matlab/Simscape, where a traditional FOC-drive with MTPA control strategy was implemented to emulate the experimental drive from Sect. IV. Simulation results are close to those from the analytical model but are not presented here because of space limitations.

A. Impact of current i_{q0}

By varying current i_{q0}, the air-gap torque $T_{em(h=hv-1=12)}$ as well as the current $I_{(hv=13)}$ maintain their typical trends, although with different p.u. values (Fig. 4); the same occurs for shaft torque $T_{sh(h)}$ and the current $I_{(hv-2=11)}$ (Fig. 5).

B. Impact of load inertia J_L

By varying the load inertia J_L while keeping the motor inertia J_m constant, the mechanical natural angular frequency $\omega_{N,mech}$ changed. In any case, the coupling damping was set to one per cent of the critical damping B=0.01B_{cr}. Like in the previous case, shaft torque harmonic $T_{sh(h=12)}$ and current harmonic $I_{(hv-2=11)}$ show the same trend (Fig. 6 and Fig. 7).

C. Impact of current loop cut-off frequency $f_{c,I}$

Another crucial parameter significantly affecting the drive response is the current loop cut-off frequency $f_{c,I}$. It was varied from 1 to 500Hz, so that both lower and higher values than $f_{N,mech}$ are tested. The drive response is shown in Fig. 8 and Fig. 9. At very low $f_{c,I}$, the amplitude trend of all the observed harmonics is almost invariable. By increasing $f_{c,I}$, both $T_{em(h)}$ and $I_{(hv)}$ are damped at any operating frequency, while $T_{sh(h)}$ and $I_{(hv-2)}$ reach only lower peak at resonance.

D. Discussion

A few rather useful conclusions can be drawn from this analysis. Obviously the mechanical resonant frequency $f_{N,mech}$ does not depend on the control loops and can be identified by

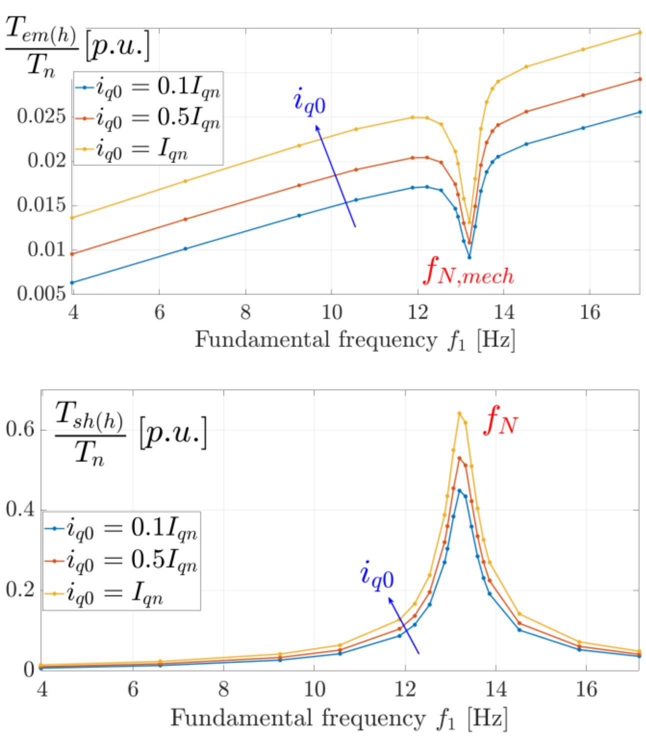

Fig. 4. Impact of i_{q0} on air-gap and shaft-torque harmonics of order h=h_v-1=12 due to a positive sequence voltage disturbance of order h_v=13. Results from the analytical model (Sect. II, A-D).

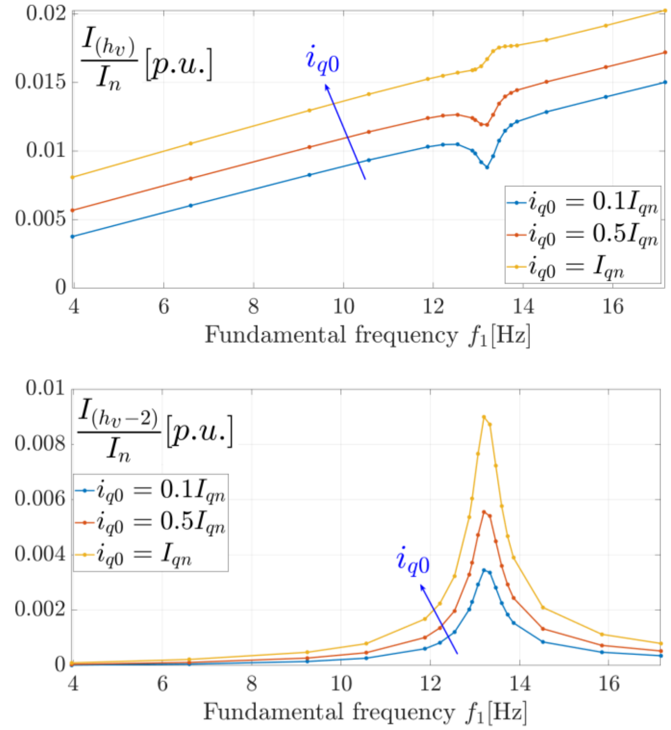

Fig. 5. Impact of i_{q0} on current harmonics of order h_v=13 and h_v-2=11 due to a positive sequence voltage disturbance of order h_v=13. Results from the analytical model.

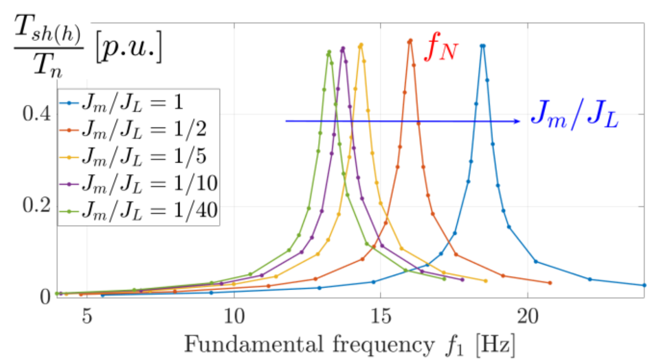

Fig. 6. Impact of J_L on the shaft-torque harmonic of order h=12, due to a positive sequence voltage disturbance of order h_v=13. Results from the analytical model.

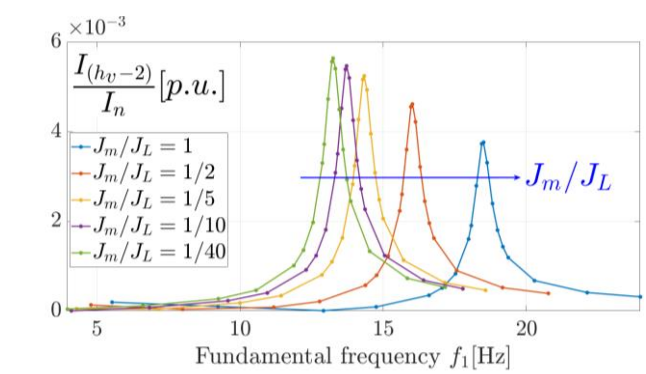

Fig. 7. Impact of load inertia J_L on current harmonic of order h_v-2=11, due to a positive sequence voltage disturbance of order h_v=13. Results from the analytical model.

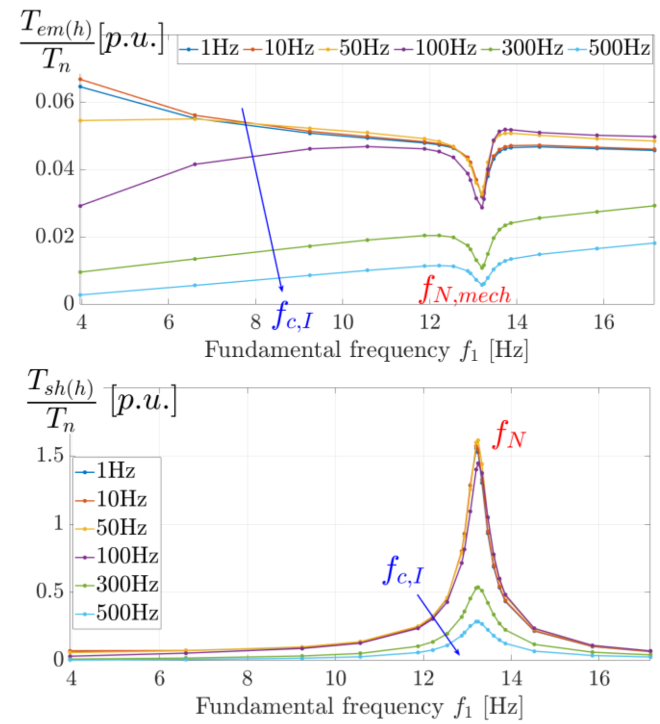

Fig. 8. Impact of current loop cut-off frequency on air-gap and shaft torque harmonics of order h=12, due to a positive sequence voltage disturbance of order h_v=13. Results from the analytical model.

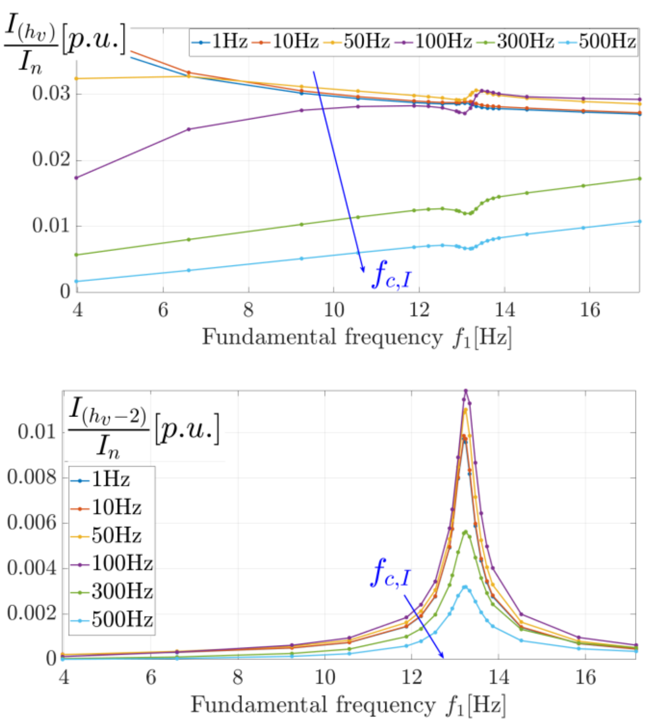

Fig. 9. Impact of $f_{c,I}$, on current harmonics of order h_v=13 and h_v-2=11, due to a positive sequence voltage disturbance of order h_v=13. Results from the analytical model.

the notch in the $T_{em(h)}$ amplitude or in i_q, given the proven approximate proportionality between $T_{em(h)}$ and i_q,. On the other hand, an exact reconstruction of $i_{q(h)}$ requires a precise measurement of the angular position θ, which can be difficult due to rotor oscillations. A simpler way of detecting $f_{N,mech}$ during characterisation tests is by searching the notch in the line current harmonic of order h_v caused by a voltage harmonic disturbance of the same order h_v. Line currents are typically measured by the drive current sensors, while a desired voltage perturbation can be applied by a dedicated routine of the drive software. The current harmonic h_v should then be monitored at different speeds. According with the top subplot in Fig. 5, however, the variation and notch in $I_{(hv)}$ may not be clearly visible.

The mechanical resonance frequency $f_{N,mech}$ can be detected by the peak of the shaft torque harmonic $T_{sh(h)}$. However, the knowledge of T_{sh} requires a torquemeter, usually not present in industrial drivetrain. The proposed analysis offers more attractive way of detecting $f_{N,mech}$ by tracking down the peak of the line current harmonic of order h_v-2 caused by a supply voltage harmonic disturbance of order h_v.

This property can be used for mechanical parameter identification but might also be exploited for future development of real-time monitoring algorithms for incipient resonance caused by VSI harmonics during the operation of the drive.

IV. Experimental Results

To verify the analytical model proposed in Sect. II, a laboratory setup was created, consisting of an SPMSM supplied by a VSI and coupled to a dc machine (Fig. 10). The main parameters of such an electrical drive are given in Appendix I; the procedure adopted to estimate the mechanical parameters is in Appendix II. The electromagnetic torque was reconstructed through the current i_q, obtained by measuring the line currents i_a, i_b, i_c (by current transducers, 50kHz bandwidth) and the motor angular position (2-channel 1024 pulse/rev incremental encoder). The shaft torque was measured directly by a rotating torque transducer AEP RT8 25Nm±0.2%, 1kHz bandwidth. To acquire all the signals, a National Instruments board NI 6225 was used with 25kHz sampling frequency and FFT analysis was performed offline to extract the relevant harmonics. The drivetrain control unit was DSP TMS320F28377D.

As a first step, the drive was characterised from a mechanical point of view: the transfer function between $T_{em(h)}$ and $T_{sh(h)}$ was experimentally derived, and the mechanical natural frequency $f_{N,mech}$ was found. The characterisation test consisted in setting the reference current $\tilde{\imath}_{q(h)} = \tilde{I}_{q(h)} \sin(2\pi f t)$ with a very low amplitude to limit the torsional oscillations and varying the frequency in the range $f \in$ [1, 400]Hz. The electromagnetic torque $T_{em(h)}$ was simply evaluated as $T_{em(h)} = n_p \cdot \psi_{PM} \cdot i_{q(h)}$ by the measured current i_q and the shaft torque $T_{sh(h)}$ was obtained by the torque meter. The harmonic amplitude of interest was evaluated offline through FFT analysis at steady state at different frequency f. In this way, the transfer function $T_{sh(h)}/T_{em(h)}$ was plotted (Fig. 11) and $f_{N,mech}$=158Hz was identified. In this test the switching frequency was kept at f_{sw}=5kHz, the current loop-bandwidth $f_{c,I}$=500Hz, and the speed loop was disabled ($k_{p\Omega}$=$k_{i\Omega}$=0).

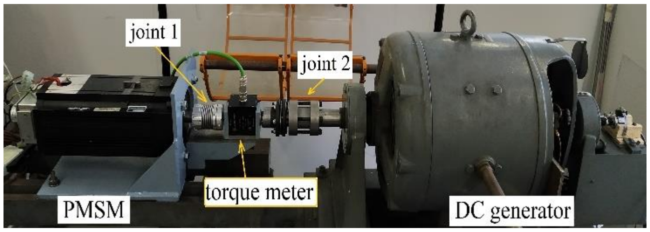

Fig. 10. Laboratory setup consisting of a PMSM connected to a dc generator through a torquemeter.

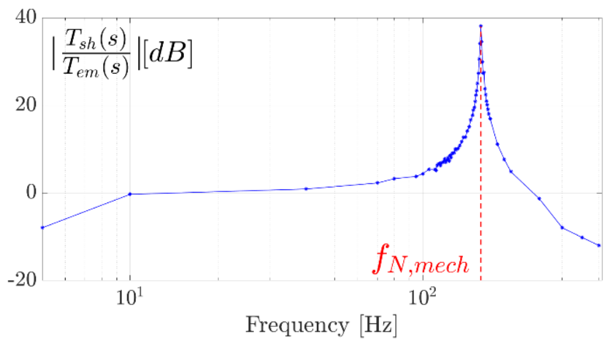

Fig. 11. Mechanical characteristic of the drivetrain in Fig. 9. Experimentally obtained transfer function between $T_{em(h)}$ and $T_{sh(h)}$.

Assuming the inertias J_m, J_L are known (see Appendix II), and B_m=B_L=0, the estimated coupling damping B and stiffness K were obtained from the measured mechanical characteristic $T_{sh(h)}/T_{em(h)}$ (in Fig. 11) through the following steps [28]:

- Identify the mechanical resonant frequency $\omega_N=2\pi f_{N,mech}$;
- Using the resonant amplification factor AF_{res} (the peak value of the measured magnitude frequency response), estimate the damping ratio: $\xi_{estim} = 1/(2 \cdot AF_{res})$;
- Estimate the coupling damping B: $B = 2 \cdot \xi_{estim} \cdot J_{eq} \cdot \omega_N$; ($J_{eq} = J_m J_L/(J_m+J_L)$);
- Estimate the coupling stiffness: $K = J_{eq} \cdot \omega_N^2$.

To validate the model and the sensitivity analysis from Sect. III, a voltage harmonic $\overline{v}_{\alpha\beta(h_v)}$ of order h_v=13 was injected into the VSI reference voltages; its amplitude was limited to avoid excessive shaft vibrations. In practice, this voltage harmonic may originate from sinusoidal PWM, either in the linear region with frequency modulation index m_f=15 (h_v= m_f – 2, see [1]) or in overmodulation with much higher m_f (h_v is one of the low order harmonics occurring in overmodulation). For the current/speed loop $f_{c,I}$=300Hz, and $f_{c,\Omega}$=0.1Hz, while f_{sw}=5kHz and i_{q0}=0.4I_{qn} were chosen. The pair of current harmonics of interest, $I_{(hv)}$ - $I_{(hv-2)}$, both computed and measured at varying fundamental frequency, are presented in Fig. 12 with respect to the rated current I_n; additionally, the electromagnetic torque $T_{em(h)}$ and the shaft torque $T_{sh(h)}$ are also reported.

Some conclusions can be drawn:

- Regarding both paired line current and torque harmonics, the theoretical values exhibit the same trend of the experimental ones and reflect the actual location of the resonance peak. Thus, the model can accurately predict the torsional resonance. Moreover, the current harmonics evaluated by the model can indicate the resonance, even in absence of a torquemeter.
- Current harmonic $I_{(hv-2)}$ shows the same trend as the shaft torque harmonic $T_{sh(h)}$, with a peak at resonance frequency. This matches the conclusions in Sect. III-D and confirms that $I_{(hv-2)}$ is a reliable indicator of incipient resonance.
- Both current harmonics $I_{(hv)}$ and $I_{(hv-2)}$ have a magnitude below one percent of the rated current value, thus it is difficult to assess whether the mismatch between calculated and test values is because of modelling or measuring issues.
- As for the electromagnetic torque harmonic $T_{em(h)}$ and shaft torque harmonic $T_{sh(h)}$, the mismatch between calculated and test values is significant, but the model overestimates the actual values, and this is in favour of safety.

The proposed analytical model deals with inverter harmonic $\bar{v}^{dist}_{\alpha\beta(h_v)}$ originating from the modulation technique, which generates torque harmonics that, in turn, excite the torsional resonance at some critical speed. Since the natural frequency is typically low, to have it excited by this type of $\bar{v}^{dist}_{\alpha\beta(h_v)}$, the drive operating speed must be rather low. The relationship between speed, excitation voltage and drive's natural frequency is commonly analysed by the well-known Campbell diagram, which identifies critical operating points.

The experimental tests here were restricted to steady-state operation, to comply with the developed mathematical model. In principle, this condition can also be interpreted as a slowly varying speed ramp.

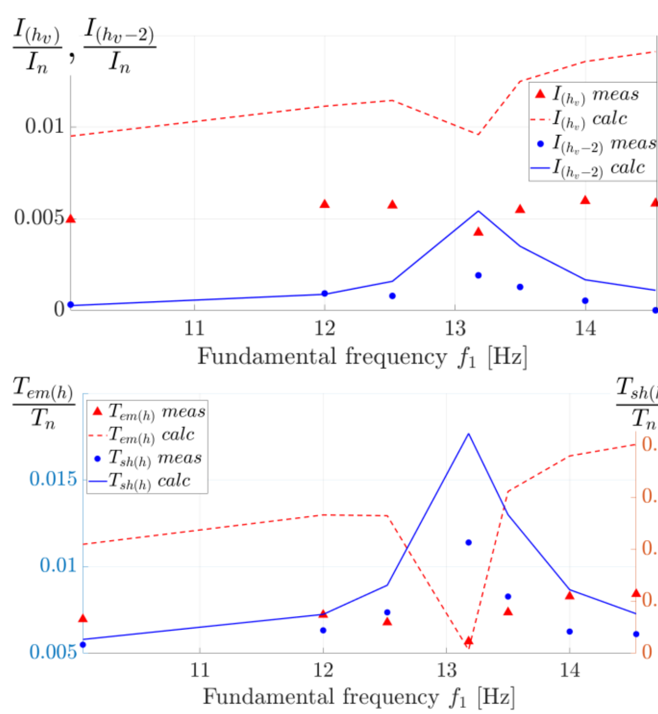

Fig. 12. Top. Current harmonics of order h_v=13 and h_v-2=11 due to a positive sequence voltage disturbance of order h_v=13. Bottom: electromagnetic torque and shaft torque of order h=h_v-1=12. Comparison between analytical and experimental results.

V. CONCLUSIONS

The paper presented an overarching mathematical model of an SPMSM drive at/about torsional resonance, accounting altogether for the electric motor characteristics, mechanical properties and drivetrain control system. The model can predict harmonics in the stator currents, electromagnetic and shaft torque at mechanical resonance caused by a voltage harmonic from the VSI modulation. The major focus was on the line current and torque harmonic interaction: the model shows that, in general, any disturbance voltage harmonic of order h_v, either applied on purpose or due to switching or overmodulation, gives rise to a pair of current harmonics of orders h_v and h_v-2 at resonance (h_v being of positive sequence), both contributing to electromagnetic and shaft torque harmonic of order $h=h_v-1$. The proposed model can accurately predict the amplitude trend of these harmonics at various operating conditions like drive speed and load. Moreover, both through a sensitivity analysis and simplified analytical approach, it was shown that the current harmonic of order h_v-2 is proportional to the shaft torque: it is nearly zero except around resonance, where it exhibits a distinctive peak. On the other hand, the current harmonic of order h_v showed the same amplitude trend of the electromagnetic torque, with an evident notch at the mechanical resonance. This amplitude similarity approach is one of the main novelties introduced in the paper. Monitoring the line current harmonics can be used for experimental identification of the drive mechanical characteristic: selected current harmonics can be excited and recorded at different frequencies. The model can also be used for forecasting the occurrence of an incipient resonance condition during drive operation. Experimental tests were performed on a small-scale SPMSM drive, which validated the system mechanical characterisation and the main model outcome. The discrepancies between computed and experimental results are deemed to be due to the relatively low current and torque values, hence may be attributed to both unmodelled parasitic effects and measuring issues.

APPENDIX I

TABLE I
ELECTRICAL AND MECHANICAL PARAMETERS OF THE SPMSM DRIVE

Electrical parameters of the SPMSM	
Rated power P_n [W]	6910
Rated torque T_n [Nm]	22
Rated frequency f_n [Hz], Rated speed Ω_n [rpm],	150; 3000
Phase resistance R [Ω]	0.393
Synchronous inductance (d,q axes) L [mH]	4.8
Permanent magnet flux ψ_{PM} [Wb]	0.165
Number of pole pairs n_p	3
Rated voltage V_n [V]	296
Current controller k_{pI}, k_{iI} (at $fc_{,I}$=300Hz)	9.4, 3740
Mechanical characteristics [24]	
Motor-side inertia J_m [kg·m^2]	$3.02 \cdot 10^{-3}$
Load-side inertia J_L [kg·m^2]	$122 \cdot 10^{-3}$
Motor-side damping B_m [Nms/rad]	$6 \cdot 10^{-4}$
Load-side damping B_L [Nms/rad]	$9 \cdot 10^{-4}$
Coupling damping B [Nms/rad]	$346 \cdot 10^{-4}$
Coupling stiffness K [Nm/rad]	2903

APPENDIX II

IDENTIFICATION OF SYSTEM MECHANICAL PARAMETERS

The mechanical parameters of the laboratory setup in Fig. 10 are shown here:

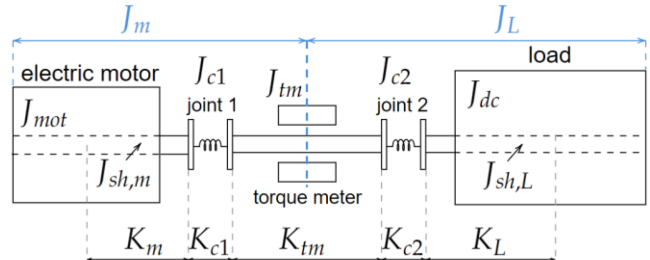

Fig. AII.1. Detailed view of the components in the experimental drive in Fig. 10.

To simplify the 5-DOF system to a 2-DOF, yet capturing the dominant natural mode, we computed the equivalent inertia and stiffness considering element series connection:

$$J_m = J_{PMSM} + J_{sh,m} + J_{c1} + J_{tm}/2 = 3.02 \cdot 10^{-3} \text{kg} \cdot \text{m}^2$$

$$J_L = J_{tm}/2 + J_{c2} + J_{sh,L} + J_{dc} = 122 \cdot 10^{-3} \text{kg} \cdot \text{m}^2$$

The inertia parameters of the single elements can be found in their datasheets or can be evaluated by assuming a simple geometrical shape like solid cylinder.

At steady state, accounting for machine viscous damping $B_m\omega_m$, $B_L\omega_L$ and constant friction torque, (3) can be written as:

$$0 = T_{em} - T_{sh} - B_m\omega_m - T_{fr,m} \qquad \text{(AII.1)}$$

$$0 = T_{sh} - T_L - B_L\omega_L - T_{fr,L} \qquad \text{(AII.2)}$$

where the shaft torque is $T_{sh} = K(\theta_m - \theta_L) - B(\omega_m - \omega_L)$.

To determine B_L and $T_{fr,L}$ we operated the drive at no load (T_L=0) with very low speed/current loop cutoff frequencies ($f_{c,I}$=1.8Hz, $\phi_{m,I}$=80° and $f_{c,\Omega}$=0.2Hz, $\phi_{m,\Omega}$=70°), so that the control system was not fast enough to follow and cancel the torque harmonics. We measured the average shaft torque at different speeds at steady state. We fitted the measured points by the least square method (LSM) and, comparing to (AII.2), obtained:

$$T_{sh}(\Omega) = B_L \cdot \Omega + T_{fr,L} = 4 \cdot 10^{-4} \cdot \Omega + 0.304 \qquad \text{(AII.3)}$$

To obtain B_m and $T_{fr,m}$, we operated the dc machine as a motor driving the PMSM at no load. We varied the system speed through the excitation winding supply and measured T_{sh} and T_{em}. Again, using the LSM to fit the measured data and (AII.1), we obtained:

$$T_{sh}(\Omega) - T_{em} = -B_m \cdot \Omega - T_{fr,m} = -9 \cdot 10^{-4} \cdot \Omega - 0.218 \qquad \text{(AII.4)}$$

REFERENCES

[1] D. Pejovski, A. Di Gerlando, G. M. Foglia, and R. Perini, "Electrical Drive in/around Torsional Resonance: Analytical Model", Proc. of the 22nd *Int. Conf. on El. Mach. ICEM*, Spain, Sept. 2022.

[2] Z. Wu, Z. Yang, K. Ding and G. He, "Transfer Mechanism Analysis of Injected Voltage Harmonic and its Effect on Current Harmonic Regulation in FOC PMSM," *IEEE Trans. on Power El.*, vol. 37, no. 1, pp. 820-829, Jan. 2022.

[3] J. Ren, X. Wang, W. Zhao and F. Liu, "Torsional Vibration Analysis and Optimization Design of the Surface PM Synchronous Machine with Reduced Torque Ripple," accepted for publication in *IEEE Trans. on Transport. Electrif.*, Oct. 2023.

[4] M. S. Khajueezadeh, S. FeizHoseini, Z. Nasiri-Gheidari and M. Behzad, "Analysis of Torsional Vibrations on the Resolver Under Eccentricity in PMSM Drive System," *IEEE Sensors Journal*, vol. 22, no. 22, pp. 21592-21599, 15 Nov.15, 2022.

[5] M. Zafarani, B. H. Jafari, and B. Akin, "Lateral and torsional vibration monitoring of multistack rotor induction motors", *IEEE Trans. on Ind. El.*, vol. 68 no. 4, pp. 3494-3505, Apr. 2021.

[6] A. F. Abouzeid, J. M. Guerrero, I. Vicente-Makazaga, I. Muniategui-Aspiazu, A. Endemaño-Isasi and F. Briz, "Torsional Vibration Suppression in Railway Traction Drives," *IEEE Access*, vol. 10, pp. 32855-32869, 2022.

[7] S. Jiang and Y. Wang, "Tangential Force Noise Reduction of Vehicular PMSM Based on Reference Harmonic Current Analytical Computation," *IEEE Trans. on Transp. Electr.*, vol. 9, no. 2, pp. 2081-2089, Jun. 2023.

[8] K. Alexander, B. Donohue, T. Feese, G. Vanderlinden, M. Kral, "Failure analysis of an MVR (mechanical vapor compressor) impeller", *Engineering Failure Analysis*, vol. 17, pp. 1345-1358, Apr. 2010.

[9] J. Vance, F. Zeidan, B. Murphy, *Machinery Vibration and Rotordynamics*, USA: John Wiley & Sons, Inc., ch. 2, pp. 51-67, 2010.

[10] I. Koene, S. Haikonen, T. Tiainen, J. Keski-Rahkonen, M. Manngård and R. Viitala, "On-Shaft Wireless Vibration Measurement Unit and Signal Processing Method for Torsional and Lateral Vibration," *IEEE/ASME Trans. on Mechatronics*, vol. 27, no. 6, pp. 5857-5868, Dec. 2022.

[11] S. H. Kia, H. Henao, and G. A. Capolino, "Torsional vibration effects on induction machine current and torque signatures in gearbox-based electromechanical system", *IEEE Trans. on Ind. El.*, vol. 56, no. 11, pp. 4689 – 4699, Nov. 2009.

[12] J. H. Leong, and Z. Q. Zhu, "A novel torsional excitation scheme for determining mechanical transfer function and natural frequencies of circumferential vibration in PM brushless machine drives", *IEEE Trans. on Magnetics*, vol. 47, no. 10, pp. 4195 – 4198, Oct. 2011.

[13] X. Jin, F. Cheng, Y. Peng, W. Qiao, and L. Qu, "Drivetrain gearbox fault diagnosis", *IEEE Ind. Appl. Magazine*, pp. 56-66, Nov./Dec. 2018.

[14] D. Yang, J. Tang, and F. Zeng, "Blade imbalance fault diagnosis of doubly fed wind turbine based on current coordinate transformation", *IEEJ Trans. on Electrical & Electronic Eng.*, vol. 14, pp. 185-191, 2018.

[15] M. Blodt, M. Chabert, J. Regnier, and J. Faucher, "Mechanical load fault detection in induction motors by stator current time-frequency analysis", IEEE Trans. on Ind. Appl., vol.42, no.6, pp. 1454-1463, Nov./Dec. 2006.

[16] Q. Han, Z. Jiang, Y. Kong, T. Wang and F. Chu, "Motor Current Model for Detecting Localized Defects in Planet Rolling Bearings," *IEEE Trans. on Ind. El.*, vol. 70, no. 9, pp. 9483-9494, Sept. 2023.

[17] A. Mahmoudi, I. Jlassi, A. J. M. Cardoso, K. Yahia and M. Sahraoui, "Inter-Turn Short-Circuit Faults Diagnosis in Synchronous Reluctance Machines, Using the Luenberger State Observer and Current's Second-Order Harmonic," *IEEE Trans. on Ind. El.*, vol. 69, no. 8, pp. 8420-8429, Aug. 2022.

[18] R. M. Rindoriya, R. K. Thakrur, B. S. Rajpurohit, R. Kumar, "Numerical and experimental analysis of torsional vibration and acoustic noise of PMSM coupled with dc generator", *IEEE Trans. on Ind. El.*, vol. 69, no.4, pp. 3345-3356, Apr. 2022.

[19] J. S. Manguelle, G. Ekemb, D. L. M. Nzongo, T. Jin, M. L. Doumbia, "A theoretical analysis of pulsating torque components in ac machines with variable frequency drives and dynamic mechanical loads", *IEEE Trans. on Ind. El.*, vol.65, no.12, pp. 9311–9324, Dec. 2018.

[20] R. Yacamini, K. S. Smith, L. Ran, "Monitoring Torsional Vibrations of Electro-Mechanical Systems Using Stator Currents", *Trans. of ASME*, vol. 120, pp. 72-79, Jan. 1998.

[21] Y. Liao, L. Ran, A. Putrus, K. S. Smith, "Evaluation of the effects of rotor harmonics in a doubly-fed induction generator with harmonic induced speed ripple", *IEEE Trans. on En. Conv.*, vol. 18, no. 4, pp. 508-515. Dec. 2003.

[22] J. Qu, P. Zhang, J. Jatskevich and C. Zhang, "Torque-Ripple Reduction of Permanent Magnet Synchronous Machine Drives Based on Novel Speed Harmonic Control at Low-Speed Operation," *IEEE Trans. on Ind. El.*, vol. 70, no. 8, pp. 7683-7694, Aug. 2023.

[23] J. Yang, J. Zhou, H. Zhou, F. Yi, D. Song and M. Dong, "High-Precision Harmonic Current Extraction for PMSM Based on Multiple Reference Frames Considering Speed Harmonics," *IEEE Trans. on Ind. El.*, vol. 70, no. 10, pp. 9764-9776, Oct. 2023.

[24] H. du Toit Mouton, B. McGrath, D. G. Holmes, R. H. Wilkinson, "One-Dimensional spectral analysis of complex PWM waveforms using superposition", *IEEE Trans. Pow. El.*, vol. 29, no. 12, pp. 6762-6778, Dec. 2014.

[25] J. Zhang, J. S. Dhupia, and C. J. Gajanayake, "Stator current analysis from electrical machines using resonance residual technique to detect faults in planetary gearboxes", *IEEE Trans. on Ind. El.*, vol. 62, no. 9, pp. 5709-5721, Sept. 2015.

[26] W. C. Gan, and L. Qiu, "Torque and velocity ripple elimination of ac permanent magnet motor control systems using the internal model principle", *IEEE/ASME Trans. on Mechatronics*, vol. 9, no. 2, pp. 436-447, Jun. 2004.

[27] D. Pejovski, A. Di Gerlando, G. M. Foglia, R. Perini, "Analytical model of Permanent Magnet Synchronous Machine in/around Resonance", Proc. of the 22nd *Int. Conf. on El. Mach. ICEM*, Spain, Sept. 2022.

[28] S. S. Rao, *Mechanical Vibrations*, 6th Ed. in SI Units, Ch. 3, pp. 316-317, Ch. 10, pp. 963-964, Pearson Education, 2018.

Dejan Pejovski received both his MS degree and PhD degree in Electrical Engineering at Politecnico di Milano, Milano, Italy in 2019 and 2023. Currently, he is a Research Fellow at Politecnico di Milano. His interests are in power electronics, electrical machines and drives.

Antonino Di Gerlando (Senior Member, IEEE) received his MS degree in electrical engineering from the Politecnico di Milano, Italy, in 1981. Currently, he is a Full Professor at the Department of Energy at Politecnico di Milano. Fields of interest: design and modelling of electrical machines, converters and drive systems. He is a senior member of IEEE, and member of the Italian Association AEIT.

Giovanni Maria Foglia received his MS degree and the PhD in electrical engineering from the Politecnico di Milano, Milano, Italy, in 1997 and 2000. Currently, he is an Assistant Professor at the Department of Energy at Politecnico di Milano, and his main field of interest is the analysis and design of PM electrical machines.

Matteo Felice Iacchetti (Senior Member, IEEE) received his PhD degree in Electrical Engineering from Politecnico di Milano in 2008. In 2014 he joined the Department of Electrical and Electronic Engineering of the University of Manchester, Manchester, UK, where he is currently a Senior Lecturer. Since October 2020 he is also as an Associate Professor at the Department of Energy of Politecnico di Milano, Milan, Italy, His main research interests include design, modelling, and control of electrical machines and drives.

Roberto Perini (Member, IEEE) received his MS degree and the PhD in electrical engineering from the Politecnico di Milano, Milano, Italy. Currently, he is an Associate Professor at the Department of Energy at Politecnico di Milano. His interests are in the design and modelling of electrical machines and power electronics.